Study of the reaction $\pi^- + {}^{12}C \rightarrow \pi^- + {}^{12}C^*(4.44\ MeV)$ at 4.5 GeV/c*

J. L. Groves,† L. E. Holloway, L. J. Koester, Jr., W.-K. Liu,‡
L. J. Nodulman,§ D. G. Ravenhall, R. L. Schult, and J. H. Smith
University of Illinois at Urbana-Champaign, Urbana, Illinois 61801
(Received 7 July 1976)

Characteristic 4.44-MeV γ rays from the first excited state of carbon were observed in coincidence with scattered 4.5-GeV/c π^- mesons in counters and wire spark chambers. The γ-ray angular distribution in the momentum-transfer frame confirms the electric quadrupole nature of the transition and reveals the polarization of the recoiling $^{12}C^*$ nucleus so that density matrix elements can be determined. A simple model with no adjustable parameters, which employs the distorted-wave impulse approximation and uses electron scattering data to obtain the nuclear transition matrix elements, predicts the angular distribution of the pions and the polarization of the $^{12}C^*$ recoils very well. However, the absolute values of the measured cross sections are only half as large as the predicted ones.

I. INTRODUCTION

The basic interactions among nucleons and mesons are usually studied by scattering mesons, nucleons, photons, or electrons from a hydrogen target in order to minimize the number of involved particles. However, the number of particles is not the only dimension of complexity. The half-integral spin and isospin of the proton target contribute to a rich mixture of quantum numbers in the final state. Rather precise measurements of polarization and momentum-transfer distributions are necessary to disentangle the desired parameters.

Stodolsky[1] pointed out that a target nucleus with good symmetry properties (e.g. zero spin and isospin) can serve as a filter to reduce the number of interfering states. ^{4}He has been used extensively for this purpose because its ground state is so simple and tightly bound. It can be observed as a recoil α particle which has no bound excited states. In the reaction[2] $\gamma + {}^4\text{He} \rightarrow \pi^0 + {}^4\text{He}$ there is no contribution from the spin-dependent and isospin-dependent term in the elementary amplitude for pion photoproduction from a single nucleon. Lubatti[3] has reviewed a number of experiments leaving the target nucleus in the ground state.

The ^{12}C nucleus has, in addition to a spinless ground state, a well-studied first excited state at 4.44 MeV. Transitions to this state have been observed by momentum analysis on the scattered particle in proton-[4-6] and pion-[7] scattering experiments, mostly at incident energies of a few hundred MeV, where the theoretical analysis is complicated by rapid changes in the energy dependence of the elementary pion-nucleon interaction. This energy dependence can be avoided by choosing incident momenta of several GeV/c, but then the relatively small momentum change in the scattered particles is hard to measure with accuracy sufficient to resolve the nuclear levels. On the other hand, the nuclear final state can be identified positively by observing the characteristic 4.44-MeV decay γ ray in coincidence with the scattered pion,[8] in which case momentum analysis is unnecessary. Such an experiment has been carried out by Scipione *et al.*[9]

The pion scattering with nuclear excitation experiment reported here was undertaken to test the theory for such reactions in a case where all the parameters are known from nucleon scattering and electron excitation. Later experiments such as $\pi + {}^{12}\text{C} \rightarrow 3\pi + {}^{12}\text{C}^*$ could then be analyzed[10,11] with some assurance that the nuclear physics is being handled correctly.

Among other nuclear processes which might be indistinguishable from the direct excitation of C* (4.44 MeV) in this poor-momentum-resolution experiment, we may consider excitation of higher-lying levels whose sequential decay process could involve the $4.44 \rightarrow 0$ phototransition. The higher $T=0$ levels have comparable excitation cross sections, and they all have overwhelmingly large branching ratios into three-α-particle decay. The 7.68-MeV, 0+ level, for example, is expected to contribute 4.44-Mev photons only $\sim 10^{-4}$ as abundantly as direct excitation of the 4.44-MeV level. Excitation of levels higher than 7.68 MeV would also lead to photons of higher energy than 4.44 MeV, and these are not seen in the photon spectrum at the level of 1% of the 4.44-MeV signal. Similarly, the first $T=1$ level at 15.1 MeV would be expected to decay predominantly to the ground state but is not seen.[12]

As an example of more complicated reactions which we could not discriminate against experimentally, there is the process $(\pi, \pi' n)$, leading to high-lying levels in ^{11}C. These could decay

through a transition from the ~5-MeV level to ground in that nucleus. The considerations of the previous paragraph militate against this possibility, but a strong argument is also the observation of a Doppler shift, to be described below.

It thus appears that ^{12}C is an unusually favorable (and possibly unique) example for a poor-momentum-resolution experiment to detect excitation to one particular nuclear excited state.

In Sec. II the experimental arrangement is described. The data analysis is discussed in Sec. III with results quoted in Sec. IV. Predictions of a multiple-scattering model are compared with the data in Sec. V.

II. EXPERIMENTAL METHOD

A. Beam, target, and γ detector

The experiment was performed in the "17° beam"[13] of the Argonne Zero Gradient Sychrotron. This beam consisted of (4.50 ± 0.04)-GeV/c negative pions with 0.5% muon, 0.8% electron, and negligible kaon contaminations. The beam (B) was defined by scintillators B_1 and B_2 (see Fig. 1) and by a 30-mm diameter hole in a veto counter A_H connected logically according to the expression $B \equiv B_1 B_2 \bar{A}_H$. This quantity was scaled and recorded for determining cross sections.

The carbon target was a 5-cm cube of graphite surrounded on four sides by veto counters A_1 and A_2 extending 10 cm parallel to the beam to eliminate events with charged fragments escaping to the sides. Downstream, the (5×5)-cm^2 beam veto A_B excluded events with straight-through tracks. The logical requirement for an interaction in the target without triggering the side counters was $B\bar{A} \equiv B_1 B_2 \bar{A}_H \bar{A}_1 \bar{A}_2 \bar{A}_B$.

An interesting event consisted of a scattered pion in coincidence with a γ ray. The γ-ray detector was a NaI (Tl) crystal 12.6 cm in diameter and 10 cm long; the last 2.4 cm was a truncated cone to the 7-cm diameter phototube face. The front face of the crystal was 15.9 cm from the target center. Data were taken with the detector placed at angles $\theta_L = 64.4°$, 90°, 111.6°, and 128.5° with respect to the z axis, which is defined as the beam direction.

The requirements on this detector were more severe than in the usual application to γ-ray spectroscopy. (1) A linear signal of fairly good resolution was essential to identify the 4.4-MeV line in the presence of a large background. (2) A fast logic signal was necessary for the coincidence requirement. (3) Both signals had to be processed with minimum delay in order that the spark chambers could be operated with a short sensitive time and still not interfere with the pulse-height analysis.

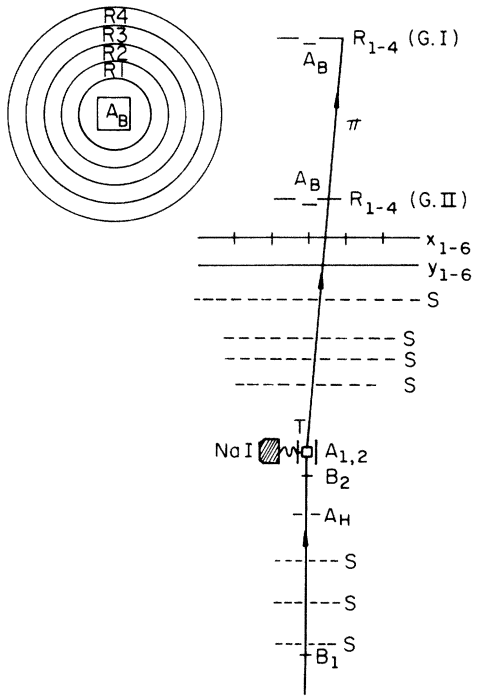

FIG. 1. Geometry of the experiment. B_1, B_2, A_H = beam-defining counters, $T = (5\text{ cm})^3$ graphite target, surrounded on four sides by veto counters $A_{1,2}$, NaI = γ detector, S = wire spark chambers, two planes each, X_{1-6}, Y_{1-6} = XY hodoscope, R_{1-4} = nested annular detectors shown in two alternate locations with beam veto A_B centered in each (see inset).

The linear signal was taken from the last dynode and the logic signal from the anode of the Dumont 6363 phototube. A two-transistor preamplifier provided current gain in each case. The anode signal was differentiated and sent to a discriminator to make the 100-nsec trigger N_I. The dynode signal was given a 100-nsec rise time to smooth out fluctuations in the photoelectrons [the decay time of NaI (Tl) scintillations is 250 nsec] and transmitted to an analog-to-digital converter[14] (ADC) operated in the peak mode. In this mode, the ADC was gated on by the event logic signal, but the gate was terminated when the analog input reached its maximum. In this way, the spark-chamber noise, which arrived some 100 nsec after the analog signal peak, was excluded from the analyzer. A 20-μsec updating inhibit gate was generated by every signal in the γ-ray counter to avoid pulse-height errors resulting from pileup. This pulse height was digitized in 300 channels.

An ideal energy calibration for the γ-ray detector is a radioactive α-beryllium neutron source, such as ^{210}Po-Be or ^{241}Am-Be. The reaction

$$^4He + {}^9Be \rightarrow {}^{12}C + n$$

frequently leaves the residual carbon nucleus in the 4.4-MeV excited state and provides a copious supply of the same γ rays observed in the experiment. These γ rays produce electron pairs, so that the first escape peak (Fig. 2) is seen 0.511 MeV below the full energy peak. Below that is a shoulder from double escape of the positron annihilation photons. Figure 3 shows that the same characteristic spectrum is obtained for γ rays in coincidence with scattered pions. The low-energy cutoff on both figures results from the logic discriminator threshold. The background pulses represent primarily random neutrons.

The scattered pions were observed in either of two ways so that the apparatus was actually used for two concurrent experiments.

B. The spark-chamber experiment

In this mode of operation the scattered pions were observed in wire-spark chambers (labeled S in Fig. 1) consisting of the three beam-defining chambers and four downstream chambers.[15] Each chamber had two wire planes with magnetostrictive readouts, one for the horizontal coordinate (X) and the other for the vertical (Y). To remove two-track ambiguities, the second beam chamber was rotated 45° about the beam axis, and the wires on the second downstream chamber were mounted at angles of $\pm\arctan(0.2)$ relative to the horizontal. The sensitive areas of the chambers were square and increased with distance from the target. All scattering angles out to 41° could be observed in these chambers, but the probability of pion scattering through such large angles was vanishingly small.

The logical trigger S for a spark-chamber event was a coincidence between a target interaction

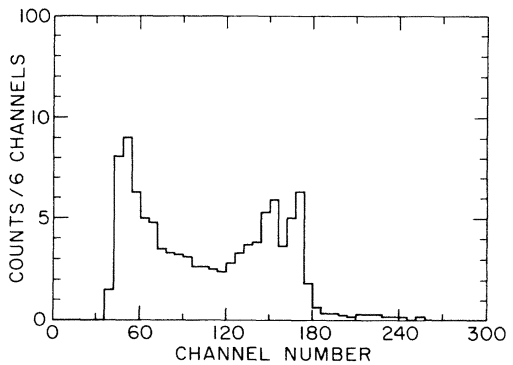

FIG. 2. Pulse-height spectrum from Po-Be source including 4.44-MeV γ rays from $^{12}C^*$. The full energy and first escape peaks are seen at the right end. The low-energy cutoff is artificial.

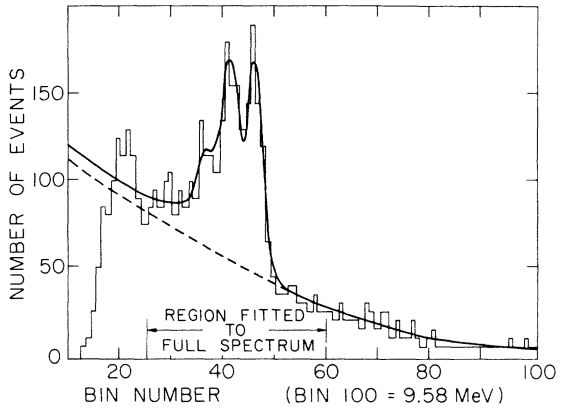

FIG. 3. Pulse-height spectrum in coincidence with pions scattered by ^{12}C (histogram). Solid curve is Monte Carlo fit, and dash curve is background subtraction.

$B\bar{A}$, a γ-ray detector count N_I, and a scattered pion X_iY_j in the XY hodoscope shown in Fig. 1. This hodoscope consisted of six (20×120)-cm^2 counters X_1–X_6 mounted side by side with their long dimensions vertical and six more Y_1–Y_6 with their long dimensions horizontal. Each set employed threshold logic to require a signal from exactly one member for pion scattering without additional particles. Thus the trigger was $S \equiv B\bar{A}X_iY_jN_I$. The coincidence resolving time for the beam counts B was 10 nsec and that for the hodoscope was 20 nsec. The logic signal N_I from the γ-ray counter was 100 nsec long.

Every counter in the hodoscope was connected to a latch gated by the fast logic. After each event, the spark locations were digitized,[15] read into the computer,[16] and stored on magnetic tape along with the contents of all the latches.

C. The ring-counter experiment

The spark-chamber apparatus described above had the advantage of covering all interesting pion-scattering angles with azimuthal measurement and multiple-track information. However, during the time intervals when the spark chambers were recovering, it was possible to obtain additional data at selected small angles with counters. To this end, a set of four nested annular counters, R_1-R_4 (inset in Fig. 1) were mounted 227 cm downstream from the target and coaxial with the beam (Geometry I). The beam veto counter A_B was at the center of the rings. Later on, the counters were moved upstream to 138 cm from the target to accept larger scattering angles (Geometry II). The ring counters were plastic scintillators 3 mm thick. Their radii and acceptances in momentum transfer squared ($-t$) are listed for the two geometries in Table I.

TABLE I. The ring counters.

Ring number	Inner and outer radii (cm)	227 cm from target Geometry I $-t$ [(GeV/c)^2]	227 cm from target Geometry I Δt [(GeV/c)^2]	138 cm from target Geometry II $-t$ [(GeV/c)^2]	138 cm from target Geometry II Δt [(GeV/c)^2]
	5.08	0.0101		0.0273	
1			0.0127		0.0342
	7.62	0.0228		0.0615	
2			0.0178		0.0478
	10.16	0.0406		0.1093	
3			0.0228		0.0615
	12.70	0.0634		0.1708	
4			0.0279		0.0751
	15.24	0.0913		0.2459	

Each time the spark chambers were fired, and as soon as they were read into the computer, a gate generator switched control from the XY hodoscope to the ring counters and inhibited the spark chambers for an 80-msec interval, then switched back to the spark-chamber logic. The logic for a ring event R was $R \equiv B\bar{A}R_iN_I$, where R_i represents any of the four ring counters. For each event trigger R, the computer recorded the γ-ray pulse height, the contents of all the latches connected to the ring counters as well as the XY hodoscope, and various identifying flags. Thus multiple-track events could be excluded from the analysis. The beam counts B defined above were gated into separate scalers during the time the spark chambers were sensitive, so that the numbers of incident pions corresponding to spark-chamber events would be recorded separately from the numbers corresponding to ring events. About 10^8 incident pions were used for the spark-chamber experiment and another 10^8 for the ring counters in each of the counter positions shown in Fig. 1.

III. DATA ANALYSIS

A. Pulse-height spectrum

The events recorded on magnetic tape were sorted into ring-counter or spark-chamber events and according to run number and pion-scattering direction. The data were thus reduced to a spectrum of pulse heights in the γ-ray detector which included the 4.44-Mev γ rays, some neutrons from breakup of the ^{12}C nucleus, and some random background.

The pulse-height response to 4.44-MeV rays was calculated with a Monte Carlo program written by Zerby and Moran,[17] which has been shown to agree with measured results in this energy region. Giannini *et al.*[18] compare this program with several others. The program specifies a right circular cylinder, whereas our crystal had a cylindrical portion 7.6 cm long and a short truncated cone at the end coupled to the phototube. We therefore assumed a cylinder with the same diameter as that of the cylindrical portion and the same total volume.

The response to a 4.44-Mev γ-ray point source on the axis of our crystal was first calculated for a 100-channel spectrum with perfect resolution. The distance from the point source to the crystal surface was the same as that from the ^{12}C target center. The calculated intrinsic efficiency was 51%, 22% of which should occur in the full energy peak.

To fit the observed spectrum, a Gaussian width proportional to the square root of the pulse height was folded into the theoretical spectrum, and a second-order polynomial background was added. A χ^2 minimization was carried out by varying parameters corresponding to the intensity, the Gaussian linewidth, and three background parameters. The solid curve on Fig. 3 shows the resulting fit to the spectrum from a typical run with the background subtraction indicated. The number of photons entering the detector is the difference between these curves divided by the intrinsic efficiency. The standard deviation of the difference is computed according to the Gaussian law for propagation of errors.

B. Doppler shift

The Doppler shift of the observed energy of the 4.44-MeV γ ray provides further identification of the C* final state. This test is possible because the C* recoil is very nearly perpendicular to the beam and is in the scattering plane, 180° opposite in azimuth, with the scattered pion. The neighboring residual nuclei, ^{11}B or ^{11}C, which may be pro-

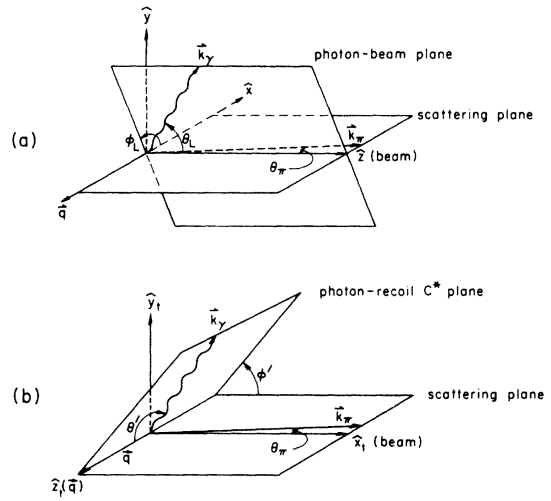

FIG. 4. (a) Laboratory coordinate system. Scattering plane contains the beam, the scattered π^- momentum $\vec{k}_\pi$, and momentum transfer $\vec{q}$. The γ-ray momentum $\vec{k}_\gamma$ at colatitude θ_L and the beam define a plane at the azimuth ϕ_L. (b) Momentum-transfer frame with z_t axis along C* recoil momentum $\vec{q}$ and x_t axis along the beam. The γ-ray momentum $\vec{k}_\gamma$ at colatitude θ' with $\vec{q}$ define a plane at the aximuth ϕ' relative to the scattering plane.

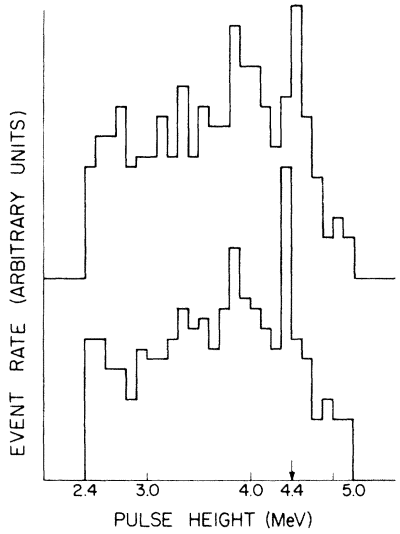

FIG. 5. Doppler shift of the γ-ray spectrum from a single run with the detector at 90° to the beam. The $^{12}C^*$ recoils toward the γ detector for the upper spectrum and away for the lower. Only the high-energy end of the spectrum is shown for clarity.

duced by ejection of a single nucleon, also emit γ rays of about 4 MeV. However, in such cases, the nucleon takes most of the momentum transfer. The ^{11}B or ^{11}C would recoil with a spectrum of energies and directions totally uncorrelated with the scattered π^-. The spectrum of an accompanying γ would be somewhat Doppler-broadened but not shifted in a sense correlated with the π^- direction.

The scattered-pion direction observed by the XY hodoscope or spark chambers determines the scattering plane and hence the recoil-C* direction [Fig. 4(a)]. Then the γ-ray pulse heights can be separated into one spectrum which should be Doppler-shifted upward because the γ is emitted along the recoil direction, and another for which the opposite is true. The two spectra compared thus in Fig. 5 were obtained concurrently during a run with the γ detector at 90° to the beam. Ring events (right or left) were selected according to the π^- azimuth determined by the XY hodoscope. Each interval on the histogram represents 96 keV and includes three bins of the pulse-height analyzer (note the spacing of the full energy and first escape peaks). The two spectra are displaced (100 ± 30) keV relative to each other in the sense consistent with the associated recoil directions.

In computing the expected shift, one must average over the allowed angles between the C* recoil and its emitted γ ray and over the spectrum of recoil volocities obtained from the scattered-π^- momentum-transfer distribution. The C* state decays with a mean life $(6\times10^{-14}\ \text{sec})$[19-21] short compared with the slowing-down time[22,23] of the ion. A small correction, less than 10%, is necessary for this attenuation. The predicted shift, 130 keV, is in satisfactory agreement with the observation.

C. Quadrupole nature of the transition

The 4.44-MeV γ ray is not emitted isotropically because the transition between the 2^+ and 0^+ states goes by electric quadrupole radiation. Observation of quadrupole characteristics in the γ-ray distribution provides a further check on the nuclear excited state. The laboratory distribution is related to the density matrix in Sec. IV B below, but the result may be stated here.

The C* spin is polarized. If the recoil direction is chosen as the quantization axis, the C* is predominantly in the $M=0$ state. The resulting azimuthal distribution, when the γ detector is set at a polar angle $\theta_L = 90°$ relative to the beam, is proportional to $(1-\cos4\phi_L)$, where ϕ_L is the azimuthal angle of the detector relative to the scattering plane. Figure 4(a) defines these angles. Each π^-C^* event is plotted as a point at the XY coordinates of the π^- in the downstream spark chamber (Fig. 6). The density of points is determined radially by the t dependence of the cross section and azimuthally by the quadrupole radiation pattern. The four-lobed azimuthal distribution represented by the above expression is clearly seen.

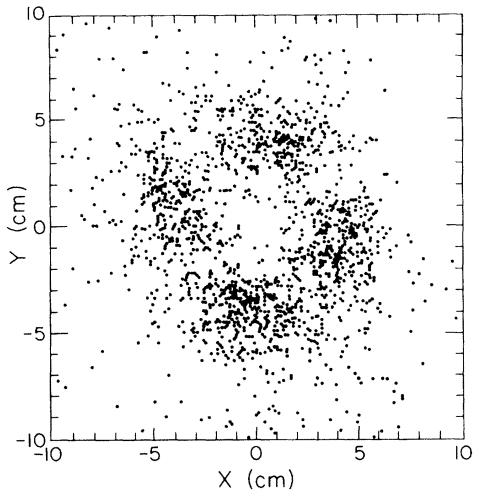

FIG. 6. Computer display of the XY distribution of scattered pions correlated with γ rays. The γ-detector position was $\theta_L = 90°$, $\phi_L = 33°$, corresponding to the minimum in the first quadrant.

D. Corrections to data

Corrections were made for (1) γ-ray losses, (2) scattered-π^- losses, and (3) secondary scattering in the target.

(1) The γ ray could interact with the carbon on its way out of the target and be absorbed or veto the event in the side counters. This attenuation probability was (10% ± 1)%, and an appropriate correction was made.

(2) The π^-, before and after scattering, traverses the entire carbon target. If it produces a δ ray that triggers an extra counter in the downstream arrays, the event is vetoed. The calculated value of δ-ray production,[24] integrated over the target thickness, depends on the minimum energy necessary to register and on the rate of energy loss of electrons in carbon. Our calculation predicts a probability of (13 ± 5)%.

During the experiment, runs were made without the extra track veto. The analysis showed that 35% of the events with an acceptable γ-ray signal had two or more particles in the downstream counters. The δ-ray production described above accounts for (13 ± 5)% of this effect, and the reaction

$$\pi^- + {}^{12}\mathrm{C} \rightarrow \pi^-\pi^+\pi^- + {}^{12}\mathrm{C}^*(4.44)$$

is known[25] to have a cross section 10% that of

$$\pi^- + {}^{12}\mathrm{C} \rightarrow \pi^- + {}^{12}\mathrm{C}^*(4.44) .$$

Thus only 12% is unaccounted for by known processes. We consider it entirely reasonable that this remaining 12% effect is due to other multipion final states involving ^{12}C*(4.44). We therefore have corrected our cross sections upward by 13% and ascribe an uncertainty of ±10% to the absolute cross section. The relative differential cross sections are unaffected by this uncertainty.

(3) The π^- may be scattered by another target nucleus either before or after the scattering event which produces the γ ray. This "secondary" scattering changes the final direction of the π^- 13% of the time. The effect of this secondary scattering is to make too many events with small and especially large angles relative to those at the most probable angle.

This correction was calculated on the basis of an 80-mb cross section for coherent scattering by the carbon nucleus varying with momentum transfer squared $[-t \text{ in}(\mathrm{GeV}/c)^2]$ as $\exp(52t)$, and a 250-mb cross section for quasielastic scattering by the nucleons varying as $\exp(7.1t)$. The appropriate subtraction was made at each scattering angle, and then all cross sections were increased by 13%.

IV. RESULTS

From the data we can determine the differential cross section for excitation, $d\sigma/dt$, and the polarization of the $J^P = 2^+$ excited state as measured by the nuclear spin density matrix $\rho_{m,m'}$ $(m,m' = -2, \ldots, +2)$. In subsection A we present the differential cross sections $d\sigma/dt$ integrated over all γ-ray directions. In subsection B we discuss the decay angular distribution of the C* state integrated over the central momentum transfer interval of the experiment.

A. Cross sections

The pions in this experiment were elastically scattered through angles $\theta_\pi \lesssim 100$ mrad, so the momentum transfer q to the C* recoil is very nearly perpendicular to the incident momentum p_π and is given very accurately by

$$q = p_\pi \theta_\pi .$$

Then

$$-t = (p_\pi \theta_\pi)^2 \qquad (1)$$

is the momentum transfer squared.

The recorded events (see III A) were binned in Δt intervals determined by the π^- scattering angles for each direction θ_L of the γ-ray detector. Since the γ rays were not emitted isotropically, the electric quadrupole radiation pattern had to be taken into account in combining all the data to compute $d\sigma/dt$ as if every emitted γ ray had been detected.

The integration over all γ-ray directions is described below in subsection B. The resulting absolute cross sections $d\sigma/dt$ are plotted vs $(-t)$ on

Fig. 7. The standard deviations are determined as in Sec. III A. The internal consistency between the spark-chamber and the ring-counter data indicates that the solid angles and detection efficiencies of the two systems for observing the scattered pions were treated consistently. The results of Scipione *et al.*[9] at 3 GeV/c are plotted for comparison. The two experiments agree within the quoted errors. The integrated cross section for this reaction is $\sigma = 1.70 \pm 0.23$ mb. We are very concerned about the disagreement by a factor 2 in absolute value between experiment and theory (see Sec. V below), but are unable to discover a source of error this large in the measurement.

B. The C* density matrix

The azimuthal information contained in the spark-chamber data can be used to sort out the populations of the various spin states of the recoiling C* nucleus. Since in the plane-wave impulse approximation no angular momentum component along the direction of the impulse can be transferred to the nucleus, we choose the momentum-transfer direction as the axis of quantization for the C* spin. The t-channel polar and azimuthal angles θ' and ϕ' of the photon are thus defined with respect to the following set of axes [Fig. 4(b)]:

$$\hat{z}_t \equiv \hat{q}_{(\text{recoil})}, \quad \hat{x}_t = \hat{p}_{\pi(\text{incident})}, \quad \hat{y}_t = \hat{z}_t \times \hat{x}_t \ .$$

The angular distribution of a spin-2 state which decays into a spin-0 state plus a photon can be written

$$W(\theta', \phi') = \sum_{m,m'} W_{m,m'}(\theta', \phi')\, \mathrm{Re}\,\rho_{m,m'} \ , \tag{2}$$

where

$$W_{m,m'}(\theta', \phi') = \frac{5}{8\pi}\left[d^2_{m,1}(\theta')d^2_{m',1}(\theta') + d^2_{m,-1}(\theta')d^2_{m',-1}(\theta')\right] \times \cos(m - m')\phi' \ .$$

The $\rho_{m,m'}$ are the C* production density matrix elements in the t-channel or recoil frame. Parity invariance of the production mechanism and of the decay interaction is assumed in order to obtain this form of the angular distribution.[26]

The transformation from the recoil frame [Fig. 4(b)] to the laboratory system with the beam along the z axis [Fig. 4(a)] can be obtained by inspection. The lab system is oriented for each event so that the negative x direction is at the same azimuth (practically coincides) with the C* recoil. Thus the unit vectors transform as follows:

$$\hat{x} = -\hat{z}_t, \quad \hat{y} = \hat{y}_t, \quad \hat{z} = \hat{x}_t \ .$$

The photon angles in the lab system are θ_L and ϕ_L. The components of a unit vector along the photon direction are

$$\begin{aligned} \sin\theta_L \cos\phi_L &= -\cos\theta' \ , \\ \sin\theta_L \sin\phi_L &= \sin\theta' \sin\phi' \ , \\ \cos\theta_L &= \sin\theta' \cos\phi' \ . \end{aligned} \tag{3}$$

In the spark-chamber experiment, each event is characterized by the values of t, θ_L, ϕ_L, and pulse height, h, in the proton counter. To extract the density matrix elements, we wish to fit the distribution of events to the expression

$$\sum_{m,m'} \frac{d\sigma}{dt}\, \rho_{m,m'} W_{m,m'}(\theta_L, \phi_L) Z(h) + \text{background},$$

where $Z(h)$ is the photon pulse-height spectrum[17] for 4.44-MeV photons incident on our NaI detector. The fitting was done by the following Fourier-transform procedure.

For each of the four settings θ_L of the photon detector, and for each value of pulse height h, we take the weighted sum of all events in the momentum-transfer interval $0.0247 < |t| < 0.0987$ (GeV/c)^2 and all ϕ_L's weighted with $\cos n\phi_L$ for $n = 0, 1, 2, 3, 4$. The resulting distributions

$$S_n(\theta_L, h) = \sum \cos n\phi_L \ ,$$

where the sum was taken over events with given θ_L and h, were fitted to the Zerby-Moran pulse-height distribution $Z(h)$ plus a polynomial back-

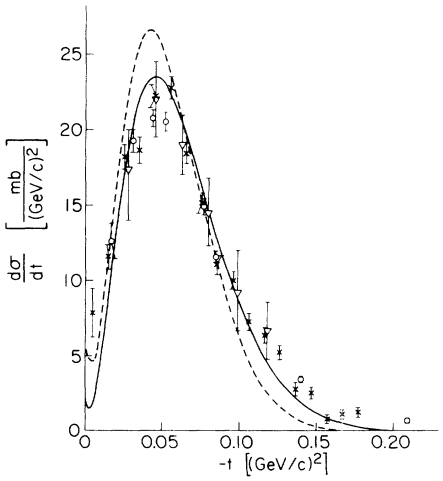

FIG. 7. Differential cross sections for the reaction $\pi^- + {}^{12}C \to \pi^- + {}^{12}C^*$. Circles: ring-counter data. Crosses: spark-chamber data. Triangles: data from Ref. 9. Solid curve is our calculation (Sec. V) divided by 2. Dashed curve is calculated with $\frac{20}{12}$ times as much absorption.

ground in h. In this way, the coefficients $b_n(\theta_L)$ were determined for the angular distribution

$$\int_{|t_{\min}|}^{|t_{\max}|} dt \frac{d\sigma}{dt} \sum_{m,m'} \rho_{m,m'} W_{m,m'}(\theta_L, \phi_L) = \sum_n b_n(\theta_L) \cos n\phi_L \ . \quad (6)$$

The spreading due to the finite γ-detector size was folded into the angular distributions, and a least-squares fit was made to determine the values of ρ_{00}, ρ_{02}, and ρ_{01}. The results are

$$\rho_{02}/\rho_{00} = 0.13 \pm 0.05 \ ,$$

$$\rho_{01}/\rho_{00} = -0.02 \pm 0.05$$

for events in the interval $0.0247 \leq |t| \leq 0.0987$ $(\mathrm{GeV}/c)^2$. The coefficients $b_n(\theta_L)$ used for this fit are plotted as points vs $\cos\theta_L$ in Fig. 8. The solid curves are the calculated values of b_n resulting from the above ratios of ρ_{02}/ρ_{00} and ρ_{01}/ρ_{00}, while the dashed curves neglect all elements except ρ_{00}. The data show too large a contribution from $n=4$ and too small a contribution from $n=2$ to be consistent with $\rho_{02}=0$.

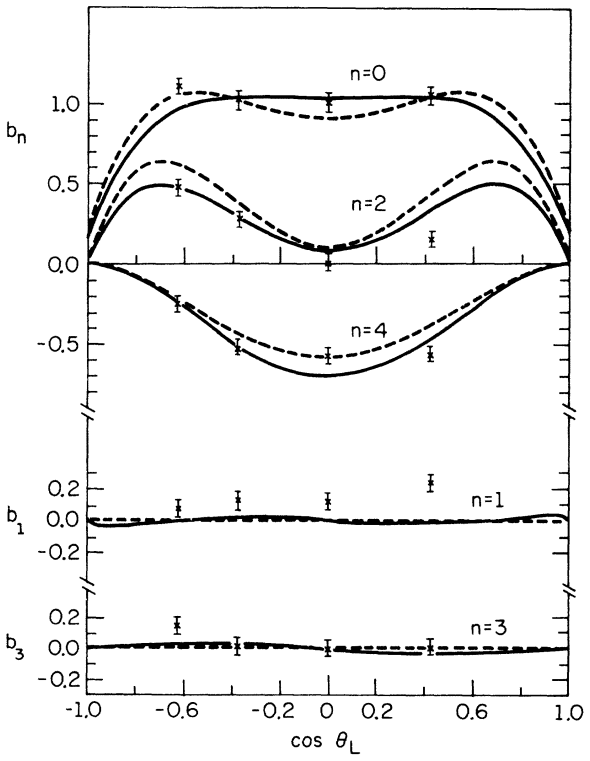

FIG. 8. Fourier coefficients of $\cos n\phi_L$ for the γ-ray distribution [Eq. (6)] in units of 0.115 mb per steradian of photon detector. The points result from Fourier analysis of the data. Solid curves are the fit with $\rho_{02} = 0.13\rho_{00}$ and $\rho_{01} = -0.02\rho_{00}$. Dashed curves have $\rho_{02} = \rho_{01} = 0$. Effects of finite counter resolution are included in the curves.

The photon angular distribution produced by the dominant matrix element ρ_{00} is

$$W_{00}(\theta', \phi') = \frac{15}{8\pi} \sin^2\theta' \cos^2\theta' \quad (7)$$

in the recoil frame, or

$$W_{00}(\theta_L, \phi_L) = \frac{15}{64\pi} \sin^2\theta_L [4 - 3\sin^2\theta_L + 4\cos^2\theta_L \cos 2\phi_L - \sin^2\theta_L \cos 4\phi_L] \quad (8)$$

in the laboratory frame. At $\theta_L = \pi/2$, this reduces to

$$W_{00}\left(\frac{\pi}{2}, \phi_L\right) = \frac{15}{64\pi}\left(1 - \cos 4\phi_L\right) , \quad (9)$$

the expression mentioned in the discussion of Fig. 6.

In the measurement of $d\sigma/dt$, averaging over ϕ_L is done by the ring counters automatically, and by the spark chambers when all events within an annular region are counted. However, the photon detector only accepts photons in a solid angle $d\Omega$ at θ_L. The probability for the photon to be emitted in an interval $d\theta_L$ at θ_L can be determined to the required precision by integrating $W_{00}(\theta_L, \phi_L)$ [Eq. (8)] over ϕ_L to obtain

$$\int_0^{2\pi} W_{00}(\theta_L, \phi_L) d\phi_L = \frac{15}{8} \sin^2\theta_L (1 - 0.75\sin^2\theta_L) .^{27}$$

The finite size of the photon detector smoothes out this distribution slightly. The fraction of all events accepted per steradian of photon detector is the geometric acceptance

$$F(\theta_L) = 0.213[0.090 + \sin^2\theta_L (1.00 - 0.72\sin^2\theta_L)] \ . \quad (10)$$

The corrected numbers of events per steradian of photon detector at each θ_L are divided by $F(\theta_L)$, summed over the four γ-detector angles, and divided by the total incident flux to obtain the values of $d\sigma/dt$ shown on Fig. 7. The solid curve of Fig. 9 compares $F(\theta_L)$ with the actual counting rates normalized at $\theta_L = 90°$.

V. THEORY

The high energies and small scattering angles used in this experiment suggest that a Glauber-type multiple-scattering[28] or distorted-wave impulse-approximation (DWIA)[29] model should be applicable. In either model the incident pion scatters off individual nucleons of the nucleus as it passes through the nucleus. Multiple scattering in the DWIA model is accounted for by calculating the distortion of the incident and outgoing pion waves

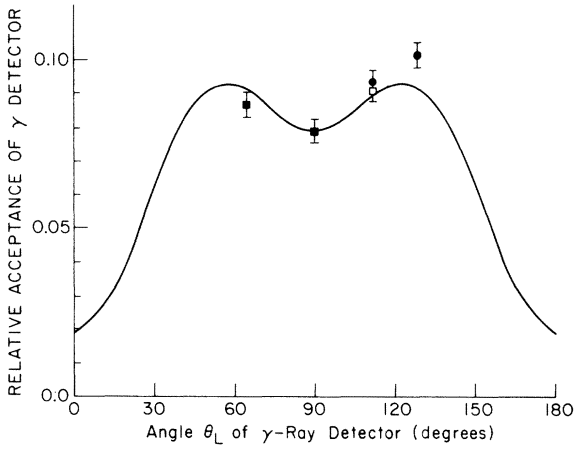

FIG. 9. Geometric acceptance of the γ detector for zero helicity C* decays. The solid curve is $F(\theta_L)$ [Eq. (10)]. Ring-counter data points are normalized at 90°. Circles are from upstream geometry, open square is from downstream geometry, and solid squares are overlapping points.

due to the elastic scattering off nucleons, represented by an optical potential

$$V(r) = \frac{2\pi}{E_\pi} f_{\pi N} \rho(r) \ . \tag{11}$$

Here $\rho(r)$ is the nucleon density distribution in the nucleus, which may be different before or after the one collision which excites the nucleus from the ground state to the final state. We designate these as ρ_i and ρ_f, respectively. The pion energy is E_π and the pion-nucleon forward elastic scattering amplitude is $f_{\pi N}$. Since high-energy pion-nucleon scattering is dominated by isoscalar exchange, the scattering from protons and neutrons is essentially the same. Furthermore, since both the ground state and the $2^+(4.44)$ state of ^{12}C are isospin singlets, the neutron distribution should be the same as the proton distribution as measured in electron scattering. Thus since we take the π-nucleon amplitude from $\pi^\pm p$ experiments and the nucleon distribution $\rho(r)$ from electron-^{12}C experiments, we have a zero-parameter prediction of the magnitude, shape, and excited-state polarization for the process measured.

Specifically, the amplitude for excitation of a C* state of helicity M is given in the DWIA model by

$$\mathfrak{M}_M = \int d^3r\, d^3r'\, \phi_\pi^{\text{out}*}(\vec{r})\psi^*_{C^*M}(\vec{r}')V(\vec{r},\vec{r}')\phi_\pi^{\text{in}}(\vec{r})\psi_C(\vec{r}') \ . \tag{12}$$

The quantities occuring in Eq. (12) are as follows:

(a) The distorted pion waves ϕ_π are given in the eikonal approximation by

$$\phi_\pi^{\text{in}}(\vec{r}) = e^{i\vec{k}_i\cdot\vec{r}} \exp\left[-\tfrac{1}{2}\sigma_{\pi N}(1-i\alpha)\int_{-\infty}^{\vec{r}} \rho_i(\vec{r}')d\vec{l}'\right] \tag{13}$$

and

$$\phi_\pi^{\text{out}}(\vec{r}) = e^{i\vec{k}_f\cdot\vec{r}} \exp\left[-\tfrac{1}{2}\sigma_{\pi N}(1+i\alpha)\int_{\vec{r}}^{\infty} \rho_f(\vec{r}')d\vec{l}'\right] . \tag{14}$$

The absorption is represented as a simple path integral along the straight-line trajectory passing through the point $\vec{r}$, in the direction $\vec{k}_i + \vec{k}_f \cong 2\vec{k}_i$.

(b) The interaction of the pion at $\vec{r}$ with the nucleon at $\vec{r}'$ is taken to be $V(\vec{r},\vec{r}') = f_{\pi N}\delta^3(\vec{r}-\vec{r}')$, representing a short-range interaction determined by $\pi^\pm p$ scattering data,

$$f_{\pi N} = \frac{k_i}{4\pi}\ \frac{\sigma_{\pi^+ p}(i+\alpha_{\pi^+ p}) + \sigma_{\pi^- p}(i+\alpha_{\pi^- p})}{2}$$

$$= \frac{k_i}{4\pi}\ \sigma_{\pi N}(i+\alpha) \ . \tag{15}$$

(Here $\alpha_{\pi^\pm p}$ is the ratio of real to imaginary parts of the forward $\pi^\pm p$ elastic scattering amplitude.) For 4.5-GeV/c pions we use[30] $\sigma_{\pi N} = 28.7$ mb and $\alpha = -0.23$.

(c) The transition nuclear density $\rho_M(r) = \psi^*_{C^*M}(r)\psi_C(r)$ is chosen to fit the electron scattering data for excitation of the $2^+(4.44)$ level. Specifically, we fit the electron excitation amplitude using Eq. (12) with no distortion of the electron waves and with the Coulomb interaction, i.e.,

$$\mathfrak{M}_M^{\text{electron}} = \frac{2E_e}{4\pi}\int d^3r\, d^3r' e^{-i\vec{k}_f\cdot\vec{r}}\psi^*_{C^*M}(\vec{r}') \times \frac{(-\frac{1}{2}e^2)}{|\vec{r}-\vec{r}'|}\psi_C(\vec{r}')e^{i\vec{k}_i\cdot\vec{r}} \ , \tag{16}$$

where $e/2$ is the average nucleon charge.

Using the transition density

$$\rho_M(\vec{r}) = A' r^2 e^{-(r/R')^2} Y_{2,M}(\theta,\phi) \ , \tag{17}$$

which gives a form factor

$$F(q^2) = Q'\left(\frac{q^2R'^2}{4}\right)\exp\left(-\frac{q^2R'^2}{4}\right), \tag{18}$$

we fit the electron data on this transition[31] with the parameter values $R' = 1.77$ fm and $Q = 4.06 \pm 0.08$, with $A' = 2Q/[\sqrt{5}\pi(R')^5]$. (These values of R' and Q correspond to a $C^* - C + \gamma$ width of 12.8 meV.) Similarly, the elastic electron-carbon scattering data were used to determine a nucleon density for the pion distorted wave,

$$\rho_i = \rho_0\left(1+\alpha'\frac{r^2}{R^2}\right)e^{-r^2/R^2} \ , \tag{19}$$

with $\rho_0 = 12/[(1+\frac{3}{2}\alpha')(\sqrt{\pi}R)^3]$, $R = 1.72$ fm, and $\alpha' = 1.12$, using the data of Ehrenberg *et al.*[32] We

assumed $\rho_f = \rho_i$ as would be given by the shell model of the nucleus.

Some characteristic features of this calculation are as follows:

(1) Neglecting the distortion of the pion waves predicts a cross section proportional to the square of the electron scattering excitation form factor [Eq. (18)]. Only the $M=0$ states is produced, and there is a zero in the pion differential cross section for forward pions because of the orthogonality of the wave functions $\psi_{C'}\psi_{C^*M}$ of the ground and excited states.

(2) The effects of including pion-wave distortion are to reduce the cross section by about a factor of 3, to admix some $M=\pm 2$ amplitudes, and partially to fill in the zero at $q^2=0$.

(3) Symmetry between the absorption of the incident and outgoing pions implies that $M=\pm 1$ amplitudes remain zero. Observation of the $M=\pm 1$ states would be a good test of $(\rho_i - \rho_f) \neq 0$.

(4) For zero-momentum transfer, the excited carbon nucleus can have no angular momentum about the beam direction (i.e., $m_z=0$, where z is the incident beam direction). Since electric quadrupole radiation in a $(2^+, m_z=0) \rightarrow 0^+$ transition vanishes for photon directions both along the z axis and in the equatorial (x, y) plane, no photons will be observed at 0° or at 90° from the beam line for momentum transfer $q^2 \rightarrow 0$.

As an estimate of the uncertainties in the theoretical calculation, we also used $\frac{11}{12}$ as much absorption (i.e., only the other 11 nucleons should influence the wave striking one nucleon) and varied the parameters R and R' within "reasonable limits." We also calculate with the Glauber multiple scattering formulas as used by Lee and McManus[28] for p-^{4}He. Predictions agree within about 5%.

As a test of the eikonal approximation, we have calculated pion-carbon elastic scattering at 1.5 GeV/c and compared the results with a partial-wave calculation using the same optical model parameters.[33] The results differ only in the bottom of the diffraction minima and then only by a few percent, indicating that the eikonal approximation is adequate.

The elastic scattering parameters were tested by comparing the model with the data of Gobbi *et al.*[34] on scattering of 2.01-GeV/c $\pi^\pm$ by ^{12}C. There is reasonable agreement with the measured total cross section, and with the small-t differential cross section, presumed to consist mainly of elastic $\pi^\pm$ ^{12}C scattering.

As a full test of the model as a description of the nuclear excitation, we have applied it to the T_{lab} = 1-GeV proton-carbon inelastic data of Friedes *et al.*[4] and Bertini *et al.*[5] and find the good agreement in magnitude and shape shown in Fig. 10. (We used $\sigma_{pN}=43.3$ mb and $\alpha=0$.)

The predicted cross section for 4.5-GeV/c pions is shown in Fig. 7, reduced in size by a factor 2. The curve includes the resolution of the counter assuming uniform efficiency over the 21° cone subtended by the NaI counter. The agreement with the data is good, indicating that the shape is acceptable, but the overall scale is too large by a factor 2. Figure 11 shows the experimental and predicted values of $\ln[(1/q^4)(d\sigma/dq^2)]$ (Tibell plot[35]) for qualitative comparison with the square of the form factor [Eq. (18)].

A further prediction of the model is the density matrix for the C* polarization,

$$\rho_{m,m'} \propto \mathfrak{M}_m \mathfrak{M}_{m'} ,$$

$$\mathrm{Tr}\rho_{m,m'} = 1 ,$$

in terms of the nucleus helicity amplitudes $\mathfrak{M}_{m'}$ [Eq. (12)]. In the helicity representation (i.e., momentum transfer to nucleus used as z axis) the calculation predicts ρ_{00} dominant, with

$$\mathrm{Re}\rho_{02} \approx 0.09\rho_{00}$$

and other terms very small. This compares with the experimental value of

$$\mathrm{Re}\rho_{02} = (0.13 \pm 0.05)\rho_{00}$$

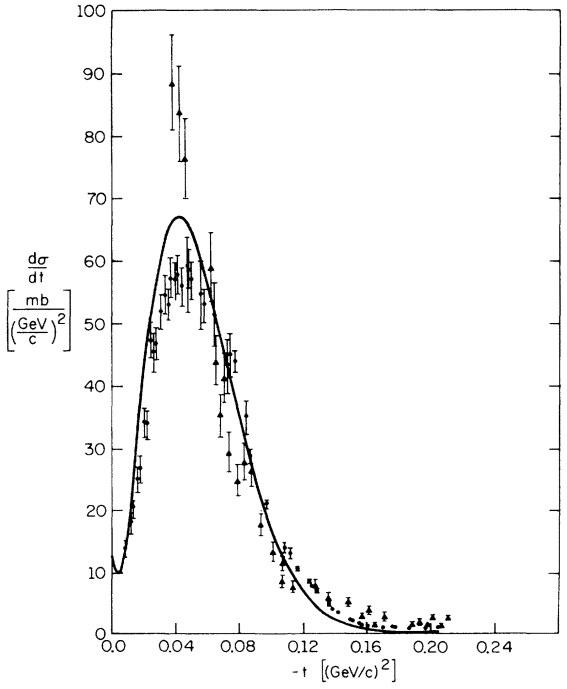

FIG. 10. Differential cross sections for the reaction $p + {}^{12}\text{C} \rightarrow p + {}^{12}\text{C}^*$ at 1.7 GeV/c. Solid curve calculated (Sec. V). Triangles are data from Ref. 4 and circles are from Ref. 5.

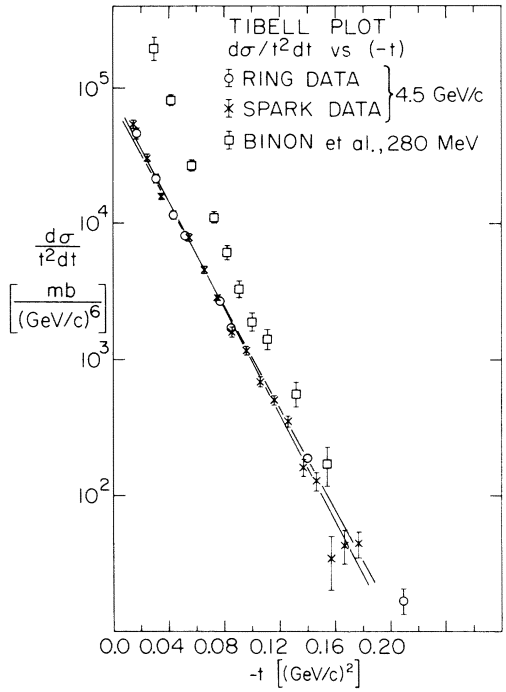

FIG. 11. Tibell plot of the cross sections divided by $q^4 = t^2$. The straight lines correspond to $b = 43$ and 45 $(\mathrm{GeV}/c)^{-2}$ in the expression $d\sigma/dt \propto t^2 \exp(bt)$. The greater slope and values of the 280-MeV data are consistent with the larger interaction radius near the (3,3) resonance.

given in Sec. IV.

To bring the theoretical cross section down to the experimental value would require some change in our ideas of how the reaction occurs. One possibility is arbitrarily to increase the pion absorption. The effect of more absorption is to reduce the size of the excitation cross section and to increase ρ_{02}. As a simple first estimate of how much extra absorption would be required, we increased absorption by a factor of $\frac{20}{12}$ and found $\rho_{02} = 0.14\rho_{00}$ and $\sigma_{\mathrm{total}}(\pi C \rightarrow \pi C^*) = 1.8$ mb, both in agreement with the data. However, the predicted shape does not fit as well as before. (See Fig. 7.) Furthermore, in our comparison with the data of Gobbi *et al.*,[34] this additional absorption increases the *elastic* $\pi + {}^{12}C$ differential cross section at $t = 0$ by a factor 2, and increases the total cross section by 40%, spoiling the agreement with the data. Simply increasing the pion absorption does not therefore appear to be the answer. It may be that unsuspected properties of the 4.44-MeV state in ^{12}C spoil the relationships of Sec. V, a, b, c between the electron-induced and pion-induced amplitudes, but we do not at present have any reasons, other than the present experiment, for doubting them.

VI. CONCLUSIONS

The cross section for excitation of the 2^+ $^{12}C^*$ (4.44) state by pion scattering has been measured by a coincidence technique. The angular distribution of the pions and the polarization of the $^{12}C^*$ are in good agreement with the results of a simple no-parameter DWIA model. However, the absolute values of the measured cross sections are about a factor 2 smaller than the theoretical predictions. The source of this discrepancy is not known. It is also present in later experiments at 6 GeV/c (Ref. 25) and in the 3-GeV/c experiment of Scipione *et al.*[9] Since the $T_L = 1$-GeV proton experiment without γ-ray coincidence does agree with the model, a test of the coincidence technique at $T_L = 1$ GeV would be helpful.

ACKNOWLEDGMENTS

The authors wish to thank J. S. Allen and M. K. Brussel for providing the sodium iodide detector. The cooperation of Russ Klem, Tony Passi, and other members of the ZGS scheduling and facilities groups helped greatly to make the experiment possible. Valuable comments by G. Ascoli regarding the expected angular distributions contributed to the experimental design. We thank Dr. J. P. Schiffer of ANL for the use of the Po-Be source.

*Work supported in part by Energy Research and Development Administration, and by the National Science Foundation.

†Present address: Department of Physics, Columbia University, New York, New York 10027.

‡Present address: Department of Chemistry, University of Waterloo, Waterloo, Ontario, Canada N2L 3G1.

§Present address: Physics Department, University of California, Los Angeles, California 90024.

[1] L. Stodolsky, Phys. Rev. 144, 1145 (1966).

[2] E. L. Goldwasser, L. J. Koester, Jr., and F. E. Mills, Phys. Rev. 95, 1692 (1954).

[3] H. J. Lubatti, Zero Gradient Synchrotron Workshops Report No. ANL/HEP 7208, Vol. 1, 1971 (unpublished), p. 213.

[4] J. L. Friedes, H. Palevsky, R. J. Sutter, G. W. Bennett, G. J. Igo, W. D. Simpson, and D. M. Corley, Nucl. Phys. A104, 294 (1967).

[5] R. Bertini, R. Beurtey, F. Brochard, G. Bruge, H. Catz, A. Chaumeaux, J. M. Durand, J. C. Faivre, J. M. Fontaine, D. Garreta, C. Gustafsson, D. Hendrie, F. Hibou, D. Legrand, J. Saudinos, and J. Thirión, Phys. Lett. 45B, 119 (1973), and private communication.

[6]G. D. Alkhazov, G. M. Amalsky, S. L. Belostotsky, A. A. Vorobyov, O. A. Domchenkov, Yu. V. Dotsenko, and V. E. Starodubsky, Phys. Lett. 42B, 121 (1972).
[7]F. Binon, P. Duteil, J. P. Garron, J. Gorres, L. Hugon, J. P. Peigneux, C. Schmit, M. Spighel, and J. P. Stroot, Nucl. Phys. B17, 168 (1970).
[8]Zero Gradient Synchrotron Workshops Report No. ANL/HEP—7208, Vol. 1, 1971 (unpublished), pp. 195f and 248ff.
[9]D. Scipione, W. Mehlhop, R. Garland, O. Piccioni, P. Kirk, P. Bowles, J. Sebek, S. Murty, H. Kobrak, J. Marraffino, and P. Allen, Phys. Lett. 42B, 489 (1972).
[10]G. Ascoli, T. J. Chapin, R. Cutler, L. E. Holloway, L. J. Koester, Jr., U. E. Kruse, L. J. Nodulman, T. Roberts, J. Tortora, B. Weinstein, and R. J. Wojslaw, Phys. Rev. Lett. 31, 795 (1973).
[11]R. T. Cutler, Phys. Rev. D 9, 676 (1974).
[12]We made a concerted effort to observe the 15.1-MeV γ ray but found no evidence for it at the level of 1% of the 4.44-MeV signal. This result seems to confirm the expectation that 4.5-GeV/c pions interact with the nucleus in an isoscalar manner.
[13]ZGS User's Handbook, Argonne National Laboratory (unpublished), p. 3.27.
[14]LeCroy Research Systems Model 243 Multimode Linear ADC, West Nyack, New York.
[15]S. W. Raither, Ph.D. thesis, University of Illinois, 1972 (unpublished).
[16]Xerox Data Systems Sigma II.
[17]C. D. Zerby and H. S. Moran, Nucl. Instrum. Methods 14, 115 (1961).
[18]M. Giannini, P. R. Olivan, and M. C. Ramarino, Nucl. Instrum. Methods 81, 104 (1970).
[19]F. Ajzenberg-Selove and T. Lauritsen, Nucl. Phys. A114, 1 (1968).
[20]E. K. Warburton, J. W. Olness, K. W. Jones, C. Chasman, R. A. Ristinen, and D. H. Wilkinson, Phys. Rev. 148, 1072 (1966).
[21]H. L. Crannell and T. A. Griffy, Phys. Rev. 136, B1580 (1964).
[22]A. L. Catz and S. Amiel, Nucl. Phys. A92, 222 (1967).
[23]L. C. Northcliffe, Annu. Rev. Nucl. Sci. 13, 67 (1963).
[24]A. D. Russell, Ph.D. thesis, University of Illinois, 1971 (unpublished).
[25]R. J. Wojslaw, Ph.D. thesis, University of Illinois, 1974 (unpublished).
[26]K. Gottfried and J. D. Jackson, Nuovo Cimento 33, 309 (1964).
[27]A similar result was found by V. V. Balashov and coworkers. See V. N. Mileev and T. V. Mishchenko, Phys. Lett. 47B, 197 (1973).
[28]R. H. Bassel and C. Wilkin, Phys. Rev. 174, 1179 (1968); H. K. Lee and H. McManus, Phys. Rev. Lett. 20, 337 (1968).
[29]C. Rogers and C. Wilkin, Lett. Nuovo Cimento 1, 575 (1971).
[30]G. Giacomelli, Report No. CERN/HERA 69-3, 1969 (unpublished), LBL, Berkeley, California.
[31]J. H. Fregeau, Phys. Rev. 104, 225 (1956); see also Ref. 21.
[32]H. F. Ehrenberg, R. Hofstadter, U. Meyer-Berkhout, D. G. Ravenhall, and S. E. Sobottka, Phys. Rev. 113, 666 (1969).
[33]We thank Dr. B. C. Clark for supplying the partial-wave calculation. See also B. C. Clark, R. L. Mercer, D. G. Ravenhall, and A. M. Saperstein, Phys. Rev. C 7, 466 (1973).
[34]B. Gobbi, W. Hakel, J. L. Rosen, and S. Shapiro, Phys. Rev. Lett. 29, 1278 (1972).
[35]G. Tibell, Phys. Lett. 28B, 638 (1969).